Precision constraints on radiative neutrino decay with CMB spectral distortion

Jelle L. Aalberts,[1] Shin'ichiro Ando,[2,1,3] Wouter M. Borg,[1] Edwin Broeils,[1] Jennypher Broeils,[1] Stephen Broeils,[1] Bradley J. Kavanagh,[2,1] Gijs Leguijt,[1] Marnix Reemst,[1] Dylan R. van Arneman,[1] and Hoang Vu[1]

[1]*Institute for Theoretical Physics, University of Amsterdam, 1098 XH Amsterdam, Netherlands*
[2]*GRAPPA Institute, University of Amsterdam, 1098 XH Amsterdam, Netherlands*
[3]*Kavli Institute for the Physics and Mathematics of the Universe (Kavli IPMU, WPI), Todai Institutes for Advanced Study, University of Tokyo, Kashiwa, Chiba 277-8583, Japan*

(Received 9 March 2018; revised manuscript received 28 May 2018; published 2 July 2018)

We investigate the radiative decay of the cosmic neutrino background and its impact on the spectrum of the cosmic microwave background (CMB) that is known to be a nearly perfect black body. We derive *exact* formulas for the decay of a heavier neutrino into a lighter neutrino and a photon, $\nu_j \to \nu_i + \gamma$, and of absorption as its inverse, $\nu_i + \gamma \to \nu_j$, by accounting for the precise form of the neutrino momentum distribution. Our calculations show that if the neutrinos are heavier than $\mathcal{O}(0.1)$ eV the exact formulas give results that differ by ∼50%, compared with approximate ones where neutrinos are assumed to be at rest. We also find that spectral distortion due to absorption is more important for heavy neutrino masses (by a factor of ∼10 going from a neutrino mass of 0.01–0.1 eV). By analyzing the CMB spectral data measured with COBE-FIRAS, we obtain lower limits on the neutrino lifetime of $\tau_{12} \gtrsim 4 \times 10^{21}$ s (95% C.L.) for the smaller mass splitting and $\tau_{13} \sim \tau_{23} \gtrsim 10^{19}$ s for the larger mass splitting. These represent up to 1 order of magnitude improvement over previous CMB constraints. With future CMB experiments such as PIXIE, these limits will improve by roughly 4 orders of magnitude. This translates to a projected upper limit on the neutrino magnetic moment (for certain neutrino masses and decay modes) of $\mu_\nu < 3 \times 10^{-11}\ \mu_B$, where μ_B is the Bohr magneton. Such constraints would make future precision CMB measurements competitive with lab-based constraints on neutrino magnetic moments.

DOI: 10.1103/PhysRevD.98.023001

I. INTRODUCTION

In the last few decades, many experiments have demonstrated that neutrinos show properties beyond the Standard Model of particle physics. They have nonzero masses and show flavor mixings as revealed by measurements of neutrino oscillations using solar, atmospheric, reactor, and accelerator neutrinos (see Refs. [1,2] for a review). There are, however, a number of important issues remaining. What is the neutrino mass hierarchy [3]? What is the *CP*-violating phase in the lepton sector [4]? How weakly do neutrinos interact with photons [5,6]? Do neutrinos decay, either radiatively or nonradiatively [7]?

Even the weak interaction predicts interactions between the neutrino and photon through a nonzero magnetic moment induced via loop corrections of the gauge boson, although its value is expected to be small [6]. We denote by μ_{ij} the magnetic moment between neutrino mass eigenstates i and j, with off-diagonal elements ($i \neq j$) representing the transition magnetic moments in radiative decay. For massive Dirac neutrinos, the value of the diagonal magnetic moment induced by loops of gauge bosons is given by [8]

$$\mu_{ii}^D = \frac{3eG_F m_i}{8\sqrt{2}\pi^2} \approx 3.2 \times 10^{-19} \left(\frac{m_i}{\mathrm{eV}}\right) \mu_B, \tag{1}$$

where μ_B is the Bohr magneton, while for the Dirac off-diagonal elements, one finds a value roughly 10^{-4} times smaller [9]. For Majorana neutrinos, one finds the magnetic moment suppressed by the ratio of the lepton and gauge boson masses:

$$\mu_{ij}^M = \frac{3eG_F m_i}{16\sqrt{2}\pi^2} \left(1 + \frac{m_j}{m_i}\right) \sum_{l=e,\mu,\tau} \mathrm{Im}[U_{lk} U_{lj}^*] \left(\frac{m_l}{m_W}\right)^2. \tag{2}$$

The current upper bound on the neutrino magnetic moment from electron-neutrino scattering experiments is $\mu_\nu < 2.8 \times 10^{-11}\ \mu_B$ [10,11]. The strongest astrophysical constraints place the bound at $\mu_\nu < 2.2 \times 10^{-12}\ \mu_B$ [12–14], well above the value expected from weak interactions alone (see Refs. [15,16] for a thorough review). However, new physics contributions could enhance the predicted magnetic moment [17–24]. In particular, Ref. [25] proposed a model with SU(2) horizontal symmetry, allowing Majorana transition neutrino magnetic

moments of order 10^{-12} μ_B while protecting the small mass of the neutrinos.

Since the neutrinos have masses that are proven to differ for different mass eigenstates, nonzero magnetic moments will induce radiative neutrino decay,

$$\nu_j \to \nu_i + \gamma, \tag{3}$$

where $m_j > m_i$. With enhanced magnetic moments, radiative neutrino decays induced by this interaction may be relevant for astrophysical systems, providing a probe of new physics in the neutrino sector. Since the mass-squared differences have been precisely measured with oscillation experiments and the absolute neutrino masses have been constrained to be below $\mathcal{O}(1)$ eV [26,27], Ref. [28] pointed out that photons emitted via neutrino decay will disturb the nearly perfect blackbody spectrum of the cosmic microwave background (CMB). By comparing with the CMB spectral data obtained with the Far Infrared Absolute Spectrophotometer (FIRAS) onboard the Cosmic Background Explorer (COBE) [29,30], Ref. [28] obtained constraints on the decay rate of $\Gamma < 2 \times 10^{-19}$–$5 \times 10^{-20}$ s^{-1}. This corresponds to $\mu_\nu \lesssim 10^{-8}$ μ_B, still much weaker than other astrophysical or lab-based constraints.

In this paper, we improve the work of Ref. [28] in several aspects. First, we argue that, if the neutrino can decay radiatively ($\nu_j \to \nu_i + \gamma$), then it is also possible that a CMB photon is absorbed by a lighter mass eigenstate of the cosmic neutrino background ν_i,

$$\nu_i + \gamma_{\rm CMB} \to \nu_j, \tag{4}$$

to create a heavier state ν_j. The cross section of this resonance process is given by

$$\sigma(E) = \frac{\pi^2}{k^2}\Gamma\delta(E - m_j), \tag{5}$$

where E is the center-of-mass energy of the initial state and k is the momentum of the center-of-mass frame [1].

Second, in contrast to approximate formulas that were derived and adopted in the literature [28,31], in which neutrinos were assumed to be at rest, we derive exact formulas by taking the neutrinos' thermal momentum distribution into account. We also include the effects of stimulated emissions for decay and Pauli blocking for both the decay and absorption. We show that all these effects can be of considerable importance in calculating the CMB spectral distortion. Therefore, neglecting these will cause a theoretical bias in the estimated lower limits on the decay lifetime.

Third, we will make projections for planned future CMB experiments. We will primarily focus on the Primordial Inflation Explorer (PIXIE) [32], which is a proposed mission to measure the CMB intensity with a higher sensitivity and wider frequency range than COBE-FIRAS. PIXIE is expected to have a sensitivity of 5 Jy/sr [33], as opposed to the COBE-FIRAS sensitivity, which is of the order of 10^4 Jy/sr [29]. We show how this improved sensitivity affects constraints on the neutrino lifetime and magnetic moment. We thus motivate future CMB experiments such as PIXIE (and the further-future PRISM experiment [34]), as probes of new physics in the neutrino sector. Finally, we note that, when obtaining the current FIRAS bounds and PIXIE sensitivities, we take into account correlations between different components of the spectral distortion such as the chemical potential as well as the residual Galactic emission.

The paper is organized as follows. In Sec. II, we present formulas for computing the intensities of microwave photons from both decay and absorption by cosmic neutrinos. The theoretical results are then compared with the CMB spectral data measured with COBE-FIRAS, and we calculate the lower limits on the decay lifetime and the upper limits on the neutrino magnetic moments for various modes and the different mass hierarchy scenarios in Sec. III. We then discuss the potential sensitivity of future CMB experiments to the neutrino radiative decay in Sec. IV and conclude the paper in Sec. V.

II. DECAY AND ABSORPTION INTENSITIES

In Sec. II A, we first derive formulas for photon intensities from both the decay of heavier neutrinos and absorption of the CMB photons by the lighter neutrinos, by assuming that the neutrinos are at rest—a reasonable approximation when the neutrino mass is much larger than the temperature of the CMB and neutrino background, on the order of 10^{-3} eV. In Sec. II B, we show exact formulas for the decay and absorption intensities, although much of the derivation is later summarized in the Appendix. In Sec. II C, we show numerical results for decay and absorption intensities, illustrating their dependence on the lightest neutrino mass, decay mode, and mass hierarchy.

A. Approximate formulation

If the neutrino can be considered at rest, according to kinematics, the energy of the absorbed CMB photon ϵ_γ (in the observer frame) is related to the neutrino masses via

$$(1 + z_a)\epsilon_\gamma = \frac{\Delta m_{ij}^2}{2m_i}, \tag{6}$$

where we have defined $m_i < m_j$, $\Delta m_{ij}^2 \equiv m_j^2 - m_i^2$, and z_a is the redshift when absorption occurs. In contrast, radiative decay follows slightly different kinematics,

$$(1 + z_d)\epsilon_\gamma = \frac{\Delta m_{ij}^2}{2m_j}, \tag{7}$$

with redshift z_d when the decay occurs. Setting $z_{a,d} = 0$ gives the maximum photon energy at which the effects of absorption or decay can be observed for given m_i, m_j.

Equation (5) shows the absorption cross section in terms of quantities in the center-of-mass frame. It is, however, more useful to use quantities in the observer frame in which the lighter neutrino ν_i is at rest and ϵ_γ is in the microwave frequency range. Then, Eq. (5) can be rewritten as

$$\sigma([1+z]\epsilon_\gamma) = \frac{\pi^2}{k^2}\Gamma\frac{m_j}{m_i}\delta\left((1+z)\epsilon_\gamma - \frac{\Delta m_{ij}^2}{2m_i}\right). \quad (8)$$

The center-of-mass momentum k for the absorption, $\nu_i + \gamma \to \nu_j$, satisfies

$$\sqrt{k^2 + m_i^2} + k = m_j, \quad (9)$$

according to energy conservation. From this, we have

$$k = \frac{\Delta m_{ij}^2}{2m_j}, \quad (10)$$

and thus

$$\sigma([1+z]\epsilon_\gamma) = \frac{4\pi^2 m_j^3\Gamma}{(\Delta m_{ij}^2)^2 m_i \epsilon_\gamma}\delta(z - z_a). \quad (11)$$

We then consider the *effective* CMB intensity due to decay and absorption, $I_{\rm dec}$ and $I_{\rm abs}$ as a function of CMB energy ϵ_γ. For a given energy ϵ_γ, there is a corresponding redshift through Eqs. (6) and (7), in which absorption and decay are allowed, respectively. These intensities can be written as a cosmological line-of-sight integral of the emissivity [35],

$$I_{\rm dec}(\epsilon_\gamma) = \frac{1}{4\pi}\int dz \frac{P_{\rm dec}([1+z]\epsilon_\gamma, z)}{H(z)(1+z)^4}, \quad (12)$$

$$I_{\rm abs}(\epsilon_\gamma) = \frac{1}{4\pi}\int dz \frac{P_{\rm abs}([1+z]\epsilon_\gamma, z)}{H(z)(1+z)^4}, \quad (13)$$

where $P_{\rm dec}$ or $P_{\rm abs}$ is the volume emissivity (energy of photons emitted per unit volume, per unit time, and per unit energy range), $H(z) = H_0\sqrt{\Omega_m(1+z)^3 + \Omega_\Lambda}$, $H_0 = 67.8\ {\rm km\,s^{-1}\,Mpc^{-1}}$ is the Hubble constant, $\Omega_m = 0.308$, and $\Omega_\Lambda = 0.692$ [26].

These emissivity functions can therefore be written as

$$\begin{aligned} P_{\rm dec}([1+z]\epsilon_\gamma, z) &= (1+z)\epsilon_\gamma n_{\nu_j}(z)\Gamma e^{-\Gamma t(z)} \\ &\quad\times [1 + f_{\rm CMB}(\epsilon_\gamma)] \\ &\quad\times \delta\left((1+z)\epsilon_\gamma - \frac{\Delta m_{ij}^2}{2m_j}\right) \\ &= (1+z)n_{\nu_j}(z)\Gamma e^{-\Gamma t(z)} \\ &\quad\times [1 + f_{\rm CMB}(\epsilon_\gamma)]\delta(z - z_d), \end{aligned} \quad (14)$$

$$\begin{aligned} P_{\rm abs}([1+z]\epsilon_\gamma, z) &= -(1+z)\epsilon_\gamma n_{\nu_i}(z) \\ &\quad\times n_{\rm CMB}([1+z]\epsilon_\gamma, z)\sigma([1+z]\epsilon_\gamma) \\ &= -\frac{2\pi^2 m_j^3\Gamma}{\Delta m_{ij}^2 m_i^2 \epsilon_\gamma}\delta(z - z_a) \\ &\quad\times n_{\nu_i}(z) n_{\rm CMB}([1+z]\epsilon_\gamma, z), \end{aligned} \quad (15)$$

where we note that the sign of $P_{\rm abs}$ is negative as it gives the suppression of the total CMB intensity. The term $[1 + f_{\rm CMB}(\epsilon_\gamma)]$ represents the stimulated emission, with $f_{\rm CMB}(\epsilon_\gamma) = (e^{\epsilon_\gamma/T_{\rm CMB}} - 1)^{-1}$ the occupation number of the CMB photons and $T_{\rm CMB} = 2.725$ K the present CMB temperature [29,30], and $n_{\rm CMB}(\epsilon_\gamma, z)$ is the CMB number density per unit energy range at ϵ_γ and z; i.e., $n_{\rm CMB}([1+z]\epsilon_\gamma, z) = (1+z)^2\epsilon_\gamma^2 f_{\rm CMB}(\epsilon_\gamma)/\pi^2$. The occupation number has no dependence on redshift, as it cancels between the energy at z, $(1+z)\epsilon_\gamma$, and the CMB temperature at z, $(1+z)T_{\rm CMB}$. We note that the effect of stimulated emission has not been taken into account in the literature [28,31], although it was acknowledged in Ref. [31]. We also assume $\Gamma t(z) \ll 1$ in the following discussions, which is well justified when the lifetime $\tau = \Gamma^{-1}$ is much larger than the age of the Universe as is the case here. By using Eqs. (14) and (15) in Eqs. (12) and (13), respectively, one can predict the effect of decay and absorption on the CMB intensity spectrum. After the δ functions collapse the redshift integral, we obtain the analytic expressions

$$I_{\rm dec}(\epsilon_\gamma) = \frac{1}{4\pi}\frac{n_{\nu_j}\Gamma}{H(z_d)}[1 + f_{\rm CMB}(\epsilon_\gamma)], \quad (16)$$

$$I_{\rm abs}(\epsilon_\gamma) = -\frac{1}{4\pi}\frac{n_{\nu_i}\Gamma}{H(z_a)}\left(\frac{m_j}{m_i}\right)^3 f_{\rm CMB}(\epsilon_\gamma), \quad (17)$$

where $n_{\nu_i} = n_{\nu_j} \approx 110\ {\rm cm^{-3}}$ are the neutrino number densities of mass eigenstates ν_i and ν_j at $z = 0$. Up to the factor for stimulated emission, Eq. (16) agrees with the formulas adopted in Ref. [28].

B. Exact formulation

Thus far, we made the approximation that both ν_i and ν_j in the initial states are at rest. This is a very good approximation when the neutrino can be regarded as nonrelativistic, which is valid in the case of $m_{i,j} \gg T_\nu = (4/11)^{1/3} T_{\rm CMB} = 1.95$ K. Otherwise, one has to take into account the momentum distribution of the neutrinos [36],

$$f_\nu(p_\nu, z) = \frac{1}{\exp[p_\nu/T_\nu(z)] + 1}, \tag{18}$$

where $T_\nu(z) = (1+z)T_\nu$ is the neutrino temperature at z.

A detailed derivation of the emissivity is summarized in the Appendix, and here we show only the results,

$$P_{\rm dec}([1+z]\epsilon_\gamma, z) = \frac{\Gamma T_\nu m_j \Delta m_{ij}^2}{4\pi^2} \frac{1 + f_{\rm CMB}(\epsilon_\gamma)}{\epsilon_\gamma} \times U\left(\frac{m_j}{(1+z)T_\nu}, \frac{\epsilon_\gamma}{T_\nu}, \frac{2(1+z)\epsilon_\gamma m_j}{\Delta m_{ij}^2}\right), \tag{19}$$

$$P_{\rm abs}([1+z]\epsilon_\gamma, z) = -\frac{2(1+z)^4}{\pi^2} \frac{\Gamma T_\nu^2 m_j^3}{(\Delta m_{ij}^2)^2} \epsilon_\gamma^2 f_{\rm CMB}(\epsilon_\gamma) \times V\left(\frac{m_i}{(1+z)T_\nu}, \frac{\epsilon_\gamma}{T_\nu}, \frac{2(1+z)\epsilon_\gamma m_i}{\Delta m_{ij}^2}\right), \tag{20}$$

for decay $(\nu_j \to \nu_i + \gamma)$ and absorption $(\nu_i + \gamma \to \nu_j)$, respectively, where

$$U(y,s,t) = \int_{\frac{y}{2}|t-\frac{1}{t}|}^{\infty} \frac{dx x}{(e^x+1)\sqrt{x^2+y^2}} \times \left[1 - \frac{1}{e^{W_-(s,t,x,y)}+1}\right], \tag{21}$$

$$V(y,s,t) = \int_{\frac{y}{2}|t-\frac{1}{t}|}^{\infty} \frac{dx x}{e^x+1} \left[1 - \frac{1}{e^{W_+(s,t,x,y)}+1}\right], \tag{22}$$

$$W_\pm(s,t,x,y) = \left[s^2 + x^2 \pm 2s\left(\sqrt{x^2+y^2} - \frac{y}{t}\right)\right]^{1/2}. \tag{23}$$

These equations are inevitably more complicated than those shown in the previous subsection but are the most accurate.

C. Results

We present numerical results for the intensity due to absorption and decay, as well as compare the approximate and exact calculations. Because it is not yet known whether the neutrino mass eigenstates are arranged in a normal hierarchy (NH) $(m_1 < m_2 \ll m_3)$ or an inverted hierarchy (IH) $(m_3 \ll m_1 < m_2)$, we include both possibilities in the calculations presented later in the paper. Throughout the paper, we adopt $\Delta m_{12}^2 = 7.53 \times 10^{-5}$ eV^2 and $\Delta m_{23}^2 = 2.5 \times 10^{-3}$ eV^2 for NH and $\Delta m_{12}^2 = 7.53 \times 10^{-5}$ eV^2 and $\Delta m_{31}^2 = 2.5 \times 10^{-3}$ eV^2 for IH [1]. We show only results for the NH in this section, noting that the results for IH are similar. The mass of the lightest neutrino mass eigenstate is m_1, and we assume a reference value of $\tau = 10^{18}$ s for the neutrino radiative decay lifetime.

Figure 1 shows the effect of decay and absorption on the CMB spectrum, in the case of transitions between m_1 and m_2, computed with the approximate formulas. We note first that the distortions to the CMB spectrum extend up to higher frequencies for lighter neutrinos, which is simply a consequence of kinematics [cf. Eqs. (7) and (6)]. We also note that the magnitude of the absorption depends on the masses of the neutrinos, with heavier neutrinos leading to a larger absorption effect. For a given photon energy today, ϵ_γ, as we decrease the mass m_i of the absorbing neutrino, the absorption must occur at earlier times (larger redshift, z_a). As we increase z_a, the period over which absorption can take place $\sim H(z_a)^{-1}$ becomes shorter, suppressing the total amount of absorptions. Decreasing m_i from 0.1 to 0.03 eV, this factor dominates over the $(m_j/m_i)^3$ scaling in the absorption intensity [Eq. (17)], and the absorption effect becomes smaller (left panel of Fig. 1).

Decreasing the lightest neutrino mass m_i further, one would expect eventually that the $(m_j/m_i)^3$ scaling would dominate over the scaling with $\sim H(z_a)^{-1} \sim (m_i/\Delta m_{ij}^2)^{3/2}$, for high z. However, at high z, the neutrino temperature is large, and the neutrino momenta, described in Eq. (18), become relevant. The nonzero neutrino momenta act to suppress the absorption cross section [Eq. (5)] which scales as k^2, where k is the center of mass from momentum. As we will see in Sec. III, the overall effect is that the absorption intensity flattens to a constant at small values of m_i. This emphasizes the importance of the exact formulation—accounting for the thermal neutrino distribution—for the correct calculation of the absorption effect.

Figures 2 and 3 compare the results of using the exact (green) and approximate (red) calculations for different neutrino masses. In each case, the left panels correspond to the decay/absorption of m_1 and m_2, while the right panels show the same for m_1 and m_3. Because Δm_{13}^2 is 2 orders of magnitude larger than Δm_{12}^2, the spectral distortions for the $3 \to 1$ mode extend up to much larger photon energies. From Fig. 2, we see the effect of the neutrino momentum distribution, which leads to a smoother cutoff in the intensity when exact formulas are used, compared to the sharp cutoff in the approximate approach. Furthermore, at low frequencies, corresponding to high-absorption redshift, the approximate absorption intensity is much larger than the exact absorption intensity. This suppression of the

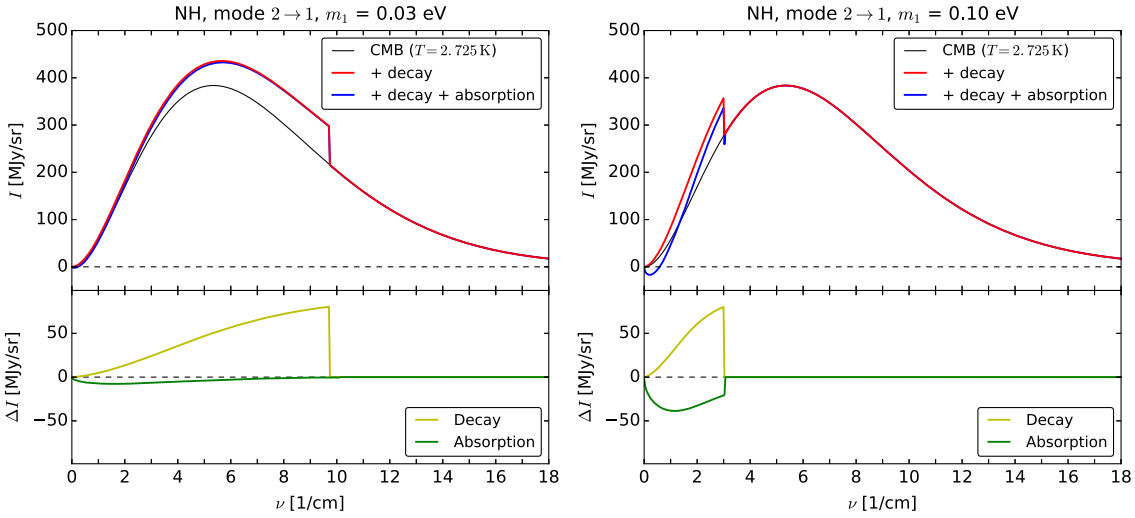

FIG. 1. Effect of neutrino decay and photon absorption on the CMB spectrum. Both panels consider NH and $\Gamma = 10^{-18}$ s^{-1} with decay/absorption between the lowest two mass eigenstates, where the lowest mass is taken to be 0.03 (left) and 0.1 eV (right). The black lines correspond to the unperturbed CMB spectrum, the red lines include the effect of photons from decaying neutrinos, and the blue lines include both decay and absorption. Here, the intensities as a function of frequency ν are calculated using the approximate formulas given in Sec. II A. In the lower panel, the CMB spectrum is not included, and only the bare intensities from decay (yellow) and absorption (green) are shown.

absorption intensity is a manifestation of the nonzero neutrino temperature, as described in the previous paragraph. Though these appear to be minor corrections, the high precision of the CMB spectral measurements means that these should be taken into account to obtain accurate limits on the neutrino lifetime.

Another effect which is observed in Figs. 2 and 3 is the impact of Pauli blocking. In the exact formalism [Eqs. (19) and (20)], the term $1-1/[e^{W_\pm(s,t,x,y)}+1]$ leads to a suppression of the decay and absorption rates when the final neutrino state is already occupied. This Pauli-blocking effect lowers the overall intensity; we see from the lower panels of Figs. 2 and 3 that the approximate intensity is always larger than the exact one, by around 50%. The stimulated emission, on the other hand, enhances the decay intensity, but the effect quickly decreases from ∼50% at 2 cm^{-1} (the lowest frequency of the FIRAS measurement) to $\lesssim$3% at >6 cm^{-1}. Therefore, the absorption and Pauli

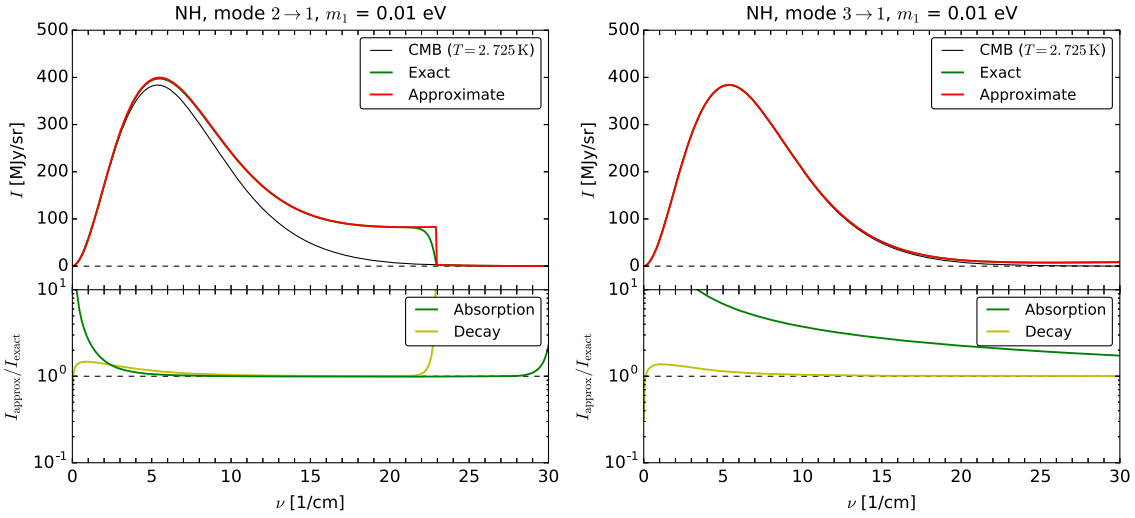

FIG. 2. Comparison between the exact and approximate neutrino decay and absorption intensities. The exact results are shown in green, and the approximate results are in red, as functions of frequency ν. Both the left- and right-hand panels use a mass of 0.01 eV for the lightest neutrino, but they consider different modes: $m_2 \leftrightarrow m_1$ (left) and $m_3 \leftrightarrow m_1$ (right). The lower panels show the ratio of the approximate and exact intensities for both absorption and decay.

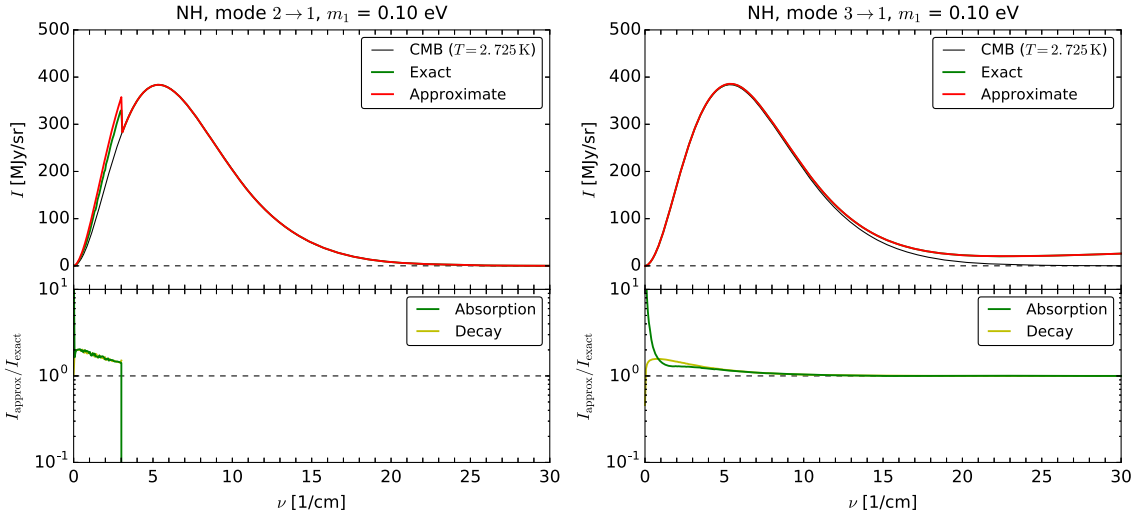

FIG. 3. The same as Fig. 2 but for a heavier neutrino mass, $m_1 = 0.1$ eV.

blocking combined should give lower intensities than were found with the formulas used in Ref. [28].

III. ANALYSIS OF THE COBE-FIRAS DATA OF CMB SPECTRUM AND LOWER LIMITS ON DECAY LIFETIME

A. Maximum likelihood analysis

COBE-FIRAS has precisely measured the CMB spectrum, in order to constrain cosmological parameters [29]. The model for the CMB intensity discussed in Ref. [29] included the effects of temperature deviations, Galactic contamination, chemical potential μ, and y distortion. Since we also include the decay and absorption, we consider an intensity I of the form

$$I = I_0 + \Delta T\frac{\partial I_\nu}{\partial T} + \mu\frac{\partial I_\nu}{\partial \mu} + G_0 I_{\rm gal} + yI_y + \Gamma_{ij}(I_{ij}^{\rm dec} + I_{ij}^{\rm abs}), \tag{24}$$

where the derivatives are to be evaluated at $T = T_0 = 2.725$ K and $\mu = 0$ and where $\Delta T \equiv T - T_0$. The index ij denotes the decay/absorption mode between the different mass eigenstates of the neutrino: $ij \in \{12, 13, 23\}$. Furthermore, G_0 is the amplitude of the Galactic contamination, y is the Kompaneets y parameter, and Γ_{ij} is the decay rate for mode ij. I_0 is a regular blackbody spectrum,

$$I_0 = I_\nu(T,\mu)|_{T=T_0,\mu=0} = \left.\frac{2h\nu^3}{e^{h\nu/T+\mu}-1}\right|_{T=T_0,\mu=0}; \tag{25}$$

$I_{\rm gal}$ is the residual Galactic contamination measured by FIRAS; I_y is given by [29,37]

$$I_y = T_0\left[\frac{h\nu}{T_0}\coth\left(\frac{1}{2}\frac{h\nu}{T_0}\right) - 4\right]\left.\frac{\partial I_\nu}{\partial T}\right|_{T=T_0,\mu=0}; \tag{26}$$

and $I_{ij}^{\rm dec}$ and $I_{ij}^{\rm abs}$ are intensities corresponding to decay and absorption, respectively, of mode ij per unit Γ.[1] Note that in reality all three modes occur simultaneously, but we find that including them all at once in the analysis would yield unnecessarily weak constraints on Γ_{ij}. This is because the masses of ν_1 and ν_2 are relatively close, resulting in degeneracy in the spectra of the modes 13 and 23. We solve this issue by focusing on one mode at a time, forcing the other two decay rates to be zero.

The parameters we are interested in are Γ_{12}, Γ_{13}, and Γ_{23}. We will constrain these by fitting the model in Eq. (24) to the FIRAS data and minimizing χ^2 as a function of the parameters ΔT, μ, G_0, y, and Γ_{ij}. The χ^2 of this model is given by

$$\chi^2 = \sum_{i,j=1}^{43}(I_i^{\rm data} - I_i^{\rm model})(C^{-1})_{ij}(I_j^{\rm data} - I_j^{\rm model}), \tag{27}$$

where $I^{\rm model}$ is given by Eq. (24), $I^{\rm data}$ is the FIRAS measurement, and C is the covariance matrix taken from Ref. [29]. The sum runs over the 43 frequency bins of FIRAS.

Our model for the intensity is defined by the parameters $\theta_a \in \{\Delta T, \mu, G_0, y, \Gamma_{ij}\}$, the best-fit values $\hat{\theta}_a$ of which are determined by solving the system of five simultaneous equations:

[1]Note that the intensities here are defined as quantities per unit *frequency* range, instead of per unit *energy* range as we defined in the previous section. We therefore have to multiply the equations in Sec. II by the Planck constant $h = 2\pi$ to compute the intensities directly compared with the FIRAS data.

$$\left.\frac{\partial\chi^2}{\partial\theta_a}\right|_{\hat{\theta}} = 0. \tag{28}$$

To estimate errors for each parameter θ_a, taking degeneracy among the parameters into account, we calculate the observed Fisher information matrix:

$$F_{ab} = \frac{1}{2}\frac{\partial^2\chi^2}{\partial\theta_a\partial\theta_b}. \tag{29}$$

The parameters $\theta_a, \theta_b \in \{\Delta T, \mu, G_0, y, \Gamma_{ij}\}$, so $\dim(F) = 5$, since we are only looking at one decay mode at a time. The derivatives in Eq. (29) are to be evaluated at the best-fit point $\hat{\theta}_a$. However, we note that, assuming the linearized intensity in Eq. (24), the Fisher information is independent of the parameters θ_a and θ_b.

The covariance between parameters θ_a and θ_b is the inverse of this matrix:

$$\mathrm{Cov}(\theta_a, \theta_b) = (F^{-1})_{ab}. \tag{30}$$

The 1σ uncertainty of a specific parameter θ_a is equivalent to the diagonal components of the covariance matrix as follows:

$$\sigma_a = \sqrt{(F^{-1})_{aa}}. \tag{31}$$

The upper limit at 95% C.L. on the parameter θ_a (corresponding to $\Delta\chi^2 \approx 2.71$) is then estimated as

$$\theta_a^{95\%} \approx \hat{\theta}_a + \sqrt{2.71}\sigma_a. \tag{32}$$

In some cases, we find that the best-fit value, $\hat{\Gamma}$, is negative, which is clearly unphysical. In this case, we assume that Eq. (29) remains a good approximation to the χ^2. The physical best fit is then at $\Gamma = 0$, and we calculate the upper limit as

$$\Gamma^{95\%} \approx \hat{\Gamma} + \sqrt{\hat{\Gamma}^2 + 2.71\sigma_\Gamma^2}. \tag{33}$$

We have checked our analysis procedure by fixing $\Gamma = 0$ and determining limits on the μ and y parameters separately. Our results are consistent with those reported in Ref. [29] ($|\mu| < 9 \times 10^{-5}$ and $|y| < 1.5 \times 10^{-5}$ at 95% C.L.).

B. Constraints on neutrino decay lifetime and transition magnetic moments

Using the approach given in the previous subsection and the FIRAS data [29], we numerically compute values for the 95% C.L. lower limit on the neutrino lifetime $\tau = 1/\Gamma$ as a function of the lowest neutrino mass. These constraints are presented in Fig. 4 for NH (left panel) and IH (right panel).

Constraints on the 13 and 23 modes are weaker than for the 12 mode by around an order of magnitude. This is as expected comparing, e.g., the left and right panels of Fig. 2, in which the distortion due to the 12 mode is clearly larger for a fixed value of τ. As outlined in Sec. II C, this is because the larger mass-squared difference in the 13 case means that the majority of the distortion appears at frequencies above the FIRAS range. For the 12 mode, the strongest constraints appear in the mass range 0.01–0.12 eV, below which the sharp spectral feature from neutrino decay lies above the FIRAS frequency range. Above ~0.12 eV, the CMB distortions from neutrino decay and absorption occur at frequencies too low to be detected by FIRAS. As pointed out in Ref. [28], the jagged shape of the limits is due to the fact that the χ^2 changes abruptly when the end point of the neutrino decay spectrum crosses into a new frequency bin.

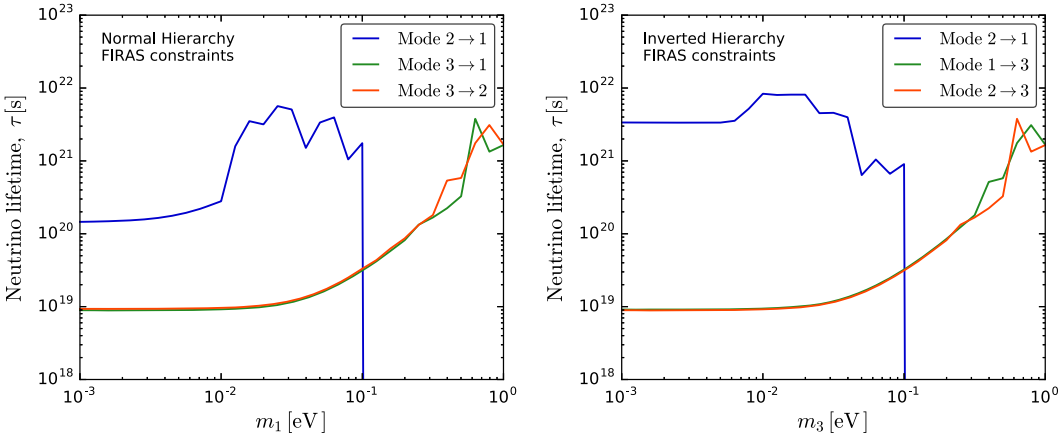

FIG. 4. 95% C.L. lower limits on radiative decay lifetime of neutrinos as a function of the lightest neutrino mass. Values of the neutrino lifetime below the solid curves are excluded by our analysis at the 95% C.L. Left panel: Results for NH, where m_1 is the lowest mass. Right panel: Results for IH where m_3 is the lowest mass.

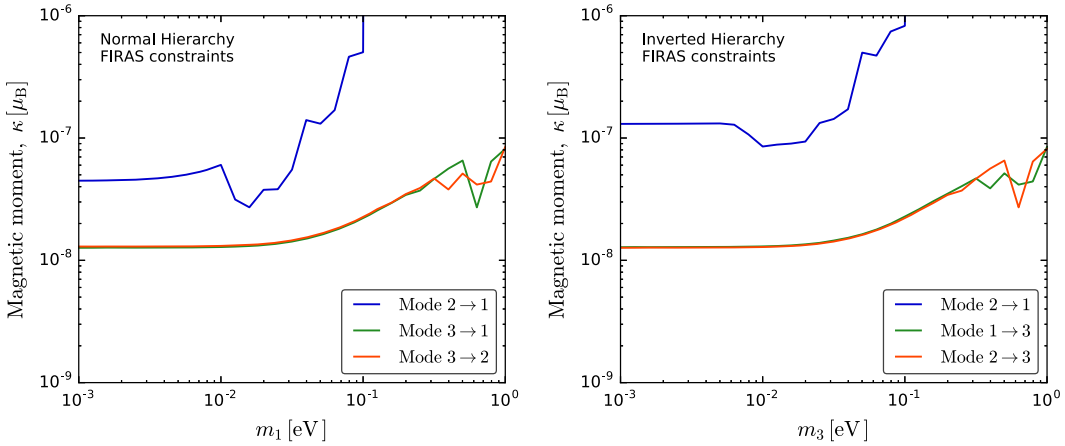

FIG. 5. 95% C.L. upper limits on the magnetic moment of neutrinos, as a function of the lightest neutrino mass. Values of the effective transition magnetic moment κ_{ij} [defined in Eq. (34)] above the solid lines are excluded by our analysis. Results shown are for NH (left panel) and IH (right panel).

We now translate our constraints on the radiative neutrino decay rate Γ into constraints on the effective neutrino magnetic moment. For neutrinos with transition magnetic and electric moments, μ_{ij} and ϵ_{ij}, respectively, we can define the effective magnetic moment $\kappa_{ij}^2 \equiv |\mu_{ij}|^2 + |\epsilon_{ij}|^2$. For a transition $\nu_j \to \nu_i + \gamma$, the decay rate induced by this magnetic moment is given by [38]

$$\Gamma_{ij} = \frac{\kappa_{ij}^2}{8\pi}\left(\frac{\Delta m_{ij}^2}{m_j}\right)^3. \tag{34}$$

The resulting constraints on κ_{ij} are shown in Fig. 5. In the case of NH (left panel), our constraints extend down to $\lesssim 10^{-8}\ \mu_B$ for the 13 and 23 modes and $\lesssim 4 \times 10^{-8}\ \mu_B$ for the 12 mode. In the case of IH (right panel), the constraints on the 12 mode are weaker by roughly a factor of 2. This is because m_1 and m_2 are larger than the case in NH, leading to a smaller decay rate for a given magnetic moment [Eq. (34)]. This dependence of the decay rate on the neutrino mass also explains why the 23 and 13 modes give stronger constraints on κ_{ij} than the 12 mode (the opposite was seen in Fig. 4).

C. Comparison to earlier work and degeneracy among parameters

We now compare our results to those previously obtained by Ref. [28]. The analysis of Ref. [28] did not take into account stimulated emission, Pauli blocking, or absorption and assumed the neutrinos to be at rest at the moment of decay. In addition, only Γ was varied in the χ^2 analysis. The difference between these results should tell us the impact of the exact calculation on the CMB spectrum as well as the importance of including additional nuisance parameters in the analysis.

When we compare our exact results to the findings in Ref. [28], we find that our results are in broad agreement with the results of Fig. 2 presented in that reference. For NH, we obtain a stronger limit for the 12 mode in the range of 10^{-2} eV $\lesssim m_\nu \lesssim 10^{-1}$ eV by about 1 order of magnitude. For IH, our bounds on the 13 and 23 modes are slightly weaker (by a factor of around 2) than the bounds found in Ref. [28] in the region 10^{-3} eV $\lesssim m_\nu \lesssim 10^{-1}$ eV. We again obtain a stronger bound on the 12 mode in the region 10^{-2} eV $\lesssim m_\nu \lesssim 10^{-1}$ eV. We emphasize that we expect our constraints to be more accurate, as we include more accurate calculations of the spectral distortions and more parameters in the analysis.

To further investigate how our results differ from the previous constraints, we have repeated our analysis, following (where possible) the analysis procedure of Ref. [28]. To do this, we used the model for the intensity,

$$I = I_0 + \Gamma_{ij} I_{ij}^{\rm dec}, \tag{35}$$

instead of the full model given in Eq. (24), fixing all the other parameters to be zero. Note that we did not include the contribution of absorption or stimulated emission and calculated the decay intensity using the approximate approach presented in Sec. II A. The uncertainty on the decay rate was then given by $\sigma_\Gamma^2 = 2(\partial^2\chi^2/\partial\Gamma^2)^{-1}$ (not taking into account the full Fisher matrix). We also adopted the mass differences and cosmological parameters stated in Ref. [28].

The resulting lower limits on τ are shown in Fig. 6, in which dashed lines are the bounds reported in Ref. [28] and solid lines show our bounds using the same analysis approach. The shape of the bounds is in close agreement. However, we notice that our bounds are around 1 order of magnitude stronger, although we have attempted to reproduce the analysis of Ref. [28] as closely as possible.

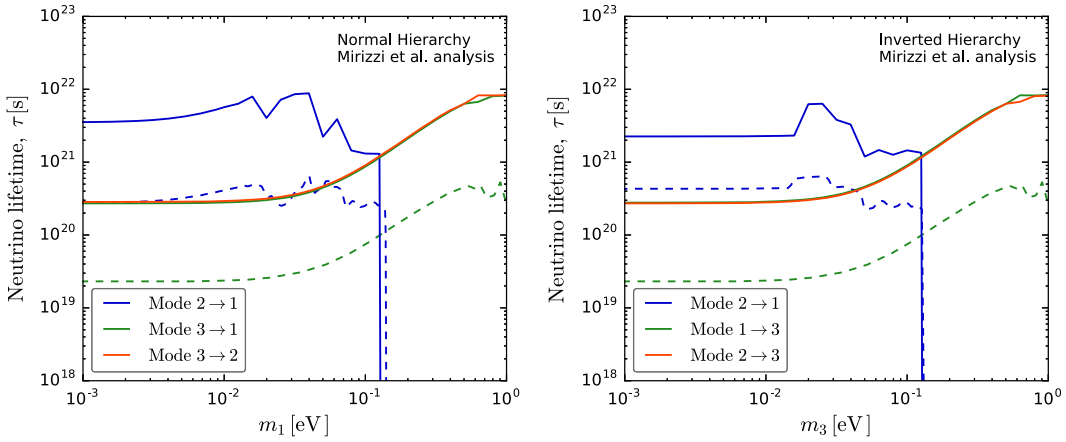

FIG. 6. 95% C.L. lower limits on the radiative decay lifetime of neutrinos, following the analysis method of Ref. [28]. These constraints were derived using approximate expressions for neutrino decay only and fixing all nuisance parameters except for Γ. Dashed lines are the limits reported by Ref. [28]. Results shown are for NH (left panel) and IH (right panel).

Unfortunately, we have not been able to find the source of this discrepancy.[2]

Lastly, when comparing our approximate bounds in Fig. 6 with the full analysis from Fig. 4, we notice that the full bounds are typically weaker by a factor of ∼30. This implies that we cannot ignore the correlation among different parameters (which are included in the full analysis). To see the effect more quantitatively, we introduce the correlation coefficients,

$$\rho(\theta_a, \theta_b) \equiv \frac{\mathrm{Cov}(\theta_a, \theta_b)}{\sigma_a \sigma_b}, \tag{36}$$

and show them between Γ_{ij} and the other parameters in Fig. 7 for the modes 12 and 13 and for both the NH and IH (those for mode 23 are almost identical to those for 13). In fact, we find very strong anticorrelation between Γ_{13} (or Γ_{23}) and the Galactic component G_0 as well as the y distortion for nearly all the masses investigated here. This is because the modification of the CMB spectrum increases as a function of the frequency without any feature and is thus indistinguishable from the Galactic residual component found in Ref. [29] up to the FIRAS errors. On the other hand, if a sharp spectral feature appears in the FIRAS frequency range (as is the case for $m_1 \in [10^{-2}, 10^{-1}]$ eV in the 12 mode), it breaks the degeneracy, and hence the anticorrelation disappears (upper left panel of Fig. 7). Indeed, we see that, comparing the full (Fig. 4) and approximate analysis (Fig. 6), the bounds in this mass range are largely unchanged between the two.

These results show that in the full analysis, including $\theta_a \in \{\Delta T, \mu, G_0, y, \Gamma_{ij}\}$, degeneracies between the parameters can substantially weaken constraints on the neutrino decay rates Γ_{ij}. While accounting for these degeneracies represents the most conservative approach, we could alternatively have chosen to fix $\mu = 0$ and $y = 0$ in the analysis. In the standard ΛCDM cosmology, we expect $y \in [10^{-7}, 10^{-6}]$, caused by heating during reionization and other heating mechanisms [39–41] and $\mu \sim \mathcal{O}(10^{-8})$, from the damping of primordial fluctuations [42]. These values lie below the FIRAS sensitivity, and so, if we assume no other sources of μ and y distortions, we could keep these parameters fixed (effectively to zero) in the analysis. The solid lines in Fig. 6 give an estimate of the limits on Γ_{ij} in this case. As we discuss in the next section, future experiments will be more sensitive to μ and y, in which case their inclusion in the analysis is unavoidable.

IV. SENSITIVITY OF FUTURE CMB EXPERIMENTS

Highly sensitive future CMB measurements will be able to measure spectral distortions to a high degree of precision. Of particular interest are μ and y distortions, briefly discussed in the previous section. These provide information about energy release at certain redshifts and therefore allow us to constrain the thermal history of the Universe [43]. A measurement of y distortions may provide information about structure formation and the epoch of reionization at $z < 10$–20, as well as allow us to probe the primordial power spectrum on small scales [44]. The decay and annihilation of particles in the prerecombination epoch ($5 \times 10^4 < z < 2 \times 10^6$) may give rise to μ distortions [45], providing sensitivity to particle lifetimes in the range $\tau \simeq 10^8$–10^{11} s. As we have explored so far in this work, particles with longer lifetimes may also distort the CMB spectrum and provide a detectable signal in future CMB experiments.

Here, we focus on the PIXIE mission, which is expected to cover a frequency range of 30 GHz (1 cm^{-1}) to 6 THz (200 cm^{-1}), using 400 channels. For this analysis, however,

[2]Reference [28] defines a reduced chi-squared test statistic but does not specify how it calculates upper limits from this, so it is difficult to reproduce its bounds exactly.

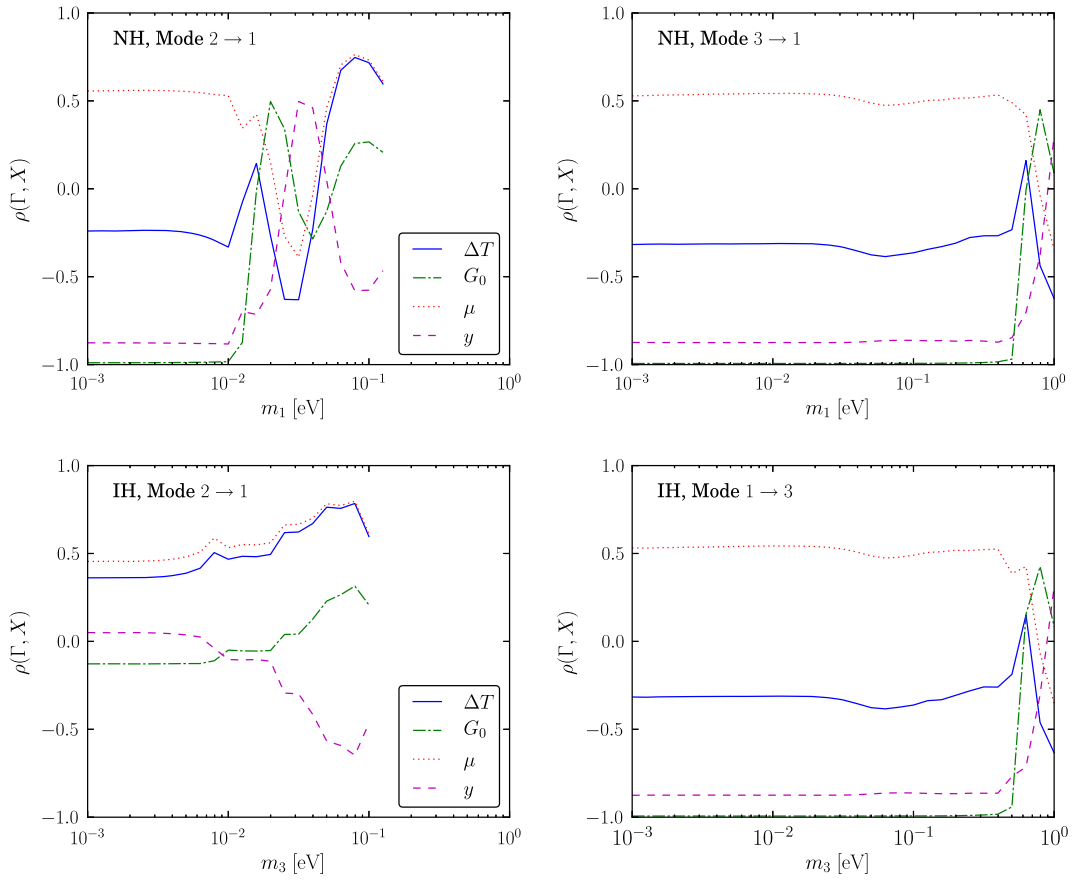

FIG. 7. Correlation coefficients $\rho(\Gamma, X)$ between the decay rate Γ and other parameters $X \in \{\Delta T, G_0, \mu, y\}$. The correlation coefficients [Eq. (36)] are shown as a function of the lightest neutrino mass, for NH (top row) and IH (bottom row) and for the modes 12 (left column) and 13 (right column).

we will only look at a range 30–750 GHz ($1 - 25$ cm^{-1}, divided into 48 frequency bins), as most of the CMB spectrum lies within this range. Furthermore, at frequencies higher than 3 THz, the spectrum is dominated by dust-emitting foregrounds that do not affect the final analysis [46].

Following closely the analysis of Sec. III, we obtain projected lower limits on the neutrino lifetime τ from the PIXIE experiment. We assume that the error on the intensity in each frequency bin is 5 Jy/sr [47] and that there are no correlations between the different frequency bins. We include the parameters $\theta_a \in \{\Delta T, \mu, G_0, y, \Gamma_{ij}\}$ in the modeled intensity, with the projected Galactic contamination taken from Ref. [46]. We also consider the ideal case in which G_0 is fixed to zero; i.e., the Galactic contamination, presumably calibrated with other wavebands, is well constrained and perfectly subtracted.

Unlike in Sec. III, the intensity spectrum has not yet been measured by PIXIE. We therefore assume that the best-fit decay rate will be $\hat{\Gamma} = 0$. Using the Fisher-matrix approach of Sec. III, we then estimate the 95% C.L. projected limit[3] on Γ as $\Gamma^{95\%} \approx 1.64\sigma_\Gamma$, where σ_Γ is defined in Eq. (31).

[3]We might also call this the projected *sensitivity* of PIXIE.

As noted in Sec. III A, in our linearized intensity model, the numerical value of the Fisher matrix does not depend on the model parameters θ_a. This means that the projection we obtain for $\Gamma^{95\%}$ does not depend on the assumed values of the nuisance parameters (although it would depend on the assumed best fit of the decay rate $\hat{\Gamma}$).

The PIXIE projected limits are shown in Fig. 8. Solid lines show the projections including parameters $\theta_a \in \{\Delta T, \mu, G_0, y, \Gamma_{ij}\}$, while dotted lines show the projection when G_0 is fixed to zero. The qualitative behavior of the bounds matches those from FIRAS, although for the 12 mode, the bounds extend to higher values of m_1 as PIXIE will probe down to lower frequencies than FIRAS. The projected limits lie in the range $\tau \gtrsim 10^{23}$–10^{25} s, representing a factor of 10^4 improvement over the FIRAS limits. This improvement arises from both a reduction of the uncertainties on the CMB intensity and from an increase in the number of frequency channels from FIRAS to PIXIE. Fixing the Galactic component to zero improves the constraints by roughly another order of magnitude (unless the spectral feature lies within the PIXIE frequency range, as is the case for masses above 10^{-2} eV in the 12 mode).

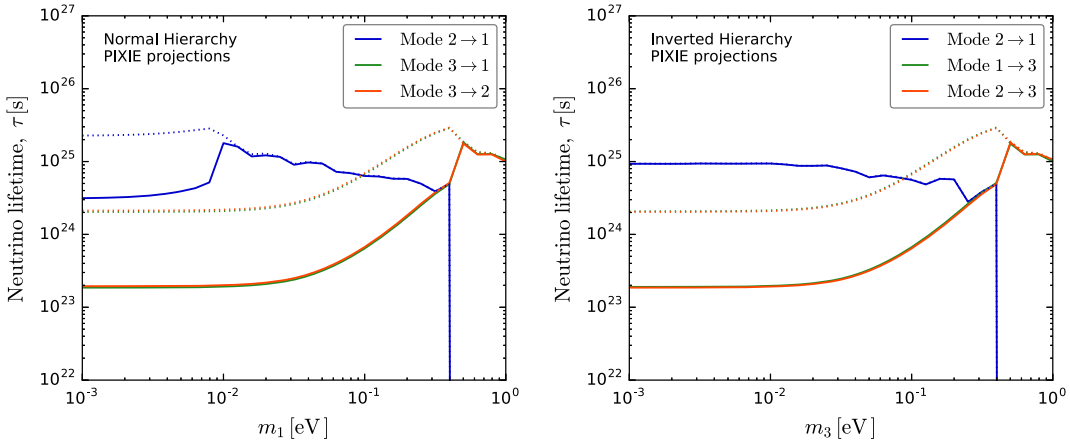

FIG. 8. Projected 95% C.L. lower limits on the radiative decay lifetime of neutrinos as a function of the lightest neutrino mass for a PIXIE-like experiment. Dotted lines correspond to the lower limits assuming that the residual Galactic contamination G_0 is fixed to zero. Left panel: Results for NH, where m_1 is the lowest mass. Right panel: Results for IH where m_3 is the lowest mass.

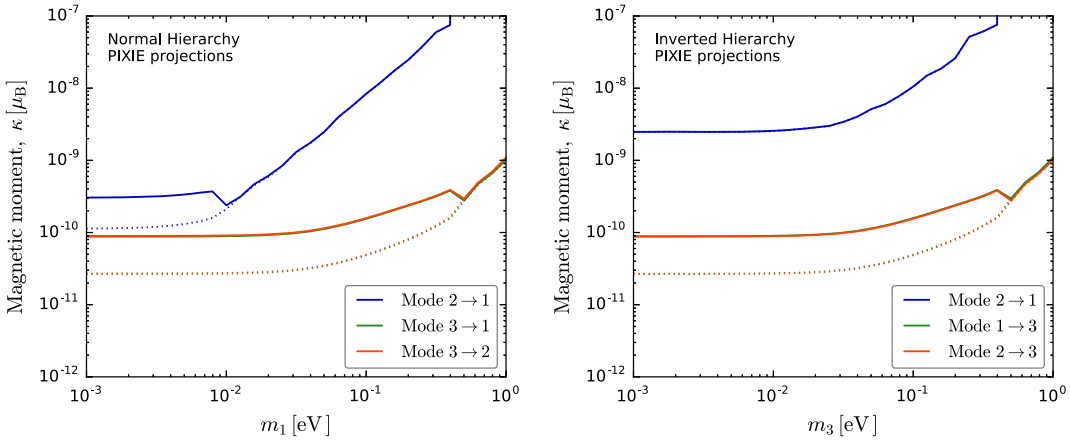

FIG. 9. Projected 95% C.L. upper limits on the magnetic moment of neutrinos, as a function of the lightest neutrino mass for a PIXIE-like experiment. The effective transition magnetic moment κ_{ij} is related to the decay rate Γ_{ij} by Eq. (34). Dotted lines correspond to the upper limits assuming that the residual Galactic contamination G_0 is fixed to zero. Results shown are for NH (left panel) and IH (right panel).

We convert the projected upper limits on the neutrino lifetime into limits on the neutrino transition magnetic and electric moments κ_{ij}. The result is shown in Fig. 9, in which again dotted lines show the case in which the Galactic component is kept fixed. The factor of 10^4 improvement in neutrino lifetime constraints translates to a factor of 10^2 improvement in the magnetic moment constraints. For the lightest neutrino masses below 0.1 eV, the limit on κ ranges from $10^{-8}\ \mu_B$ down to $3 \times 10^{-11}\ \mu_B$, depending on the hierarchy and assumptions about Galactic contamination. In particular, we note that for the 23 mode, lightest neutrino mass lower than 10^{-2} eV, and minimal Galactic contamination, constraints from a PIXIE-like experiment may be competitive with the best lab-based ν–e scattering experiments (cf. constraints from BOREXINO giving $\mu_\nu < 2.8 \times 10^{-11}\ \mu_B$ [48] at 90% C.L.).

V. CONCLUSIONS

In this work, we have presented updated constraints on the neutrino radiative decay lifetime τ from FIRAS measurements of the CMB intensity spectrum, introducing a number of refinements compared to previous work [28]. We included spectral distortions from photon absorption by neutrinos (not only from neutrino decays) as well as calculated decay and absorption rates, taking into account the momentum distribution of the cosmic neutrino background. In our analysis, we simultaneously fit the neutrino decay rate $\Gamma = 1/\tau$ along with other nuisance parameters, including the temperature deviation ΔT, μ and y distortions, and the residual Galactic contamination G_0. These led to more accurate and robust limits than previously presented.

We found that the effects of absorption and decay are comparable for neutrino masses $\mathcal{O}(0.1)$ eV and larger. We

also found that the approximate formalism (assuming that the cosmic neutrinos are at rest) may overestimate the spectral distortions by around 50%. Finally, we found strong anticorrelation between the decay rate Γ and the other nuisance parameters in the analysis, weakening the constraints on the neutrino lifetime unless a clear spectral feature was produced in the FIRAS frequency range (as was that case in which the lightest mass lay in $[10^{-2}, 10^{-1}]$ eV for the 12 mode). While these effects should tend to weaken our constraints, we in fact found stronger constraints than previous analyses [28], in some cases by around an order of magnitude, although the source of this discrepancy was not clear. In particular, we found $\tau_{12} \gtrsim 4 \times 10^{21}$ s for the 12 decay mode in the normal hierarchy and $\tau_{12} \gtrsim 10^{22}$ s in the inverted hierarchy. For the 13 and 23 modes, there were no sharp spectral features in the FIRAS frequency range, leading to weaker limits, $\tau_{13} \sim \tau_{23} \gtrsim 10^{19}$ s. The corresponding constraints on the neutrino magnetic moment lay in the range $10^{-8} - 10^{-7}\ \mu_B$.

We have also explored projected constraints from future precision CMB spectral measurements, focusing on the proposed PIXIE experiment [32]. With an improvement in measurement sensitivity of around 3 orders of magnitude compared to FIRAS, PIXIE should be able to constrain the radiative decay lifetime of the neutrino at the level of $\tau \gtrsim 10^{23}$–10^{25} s depending on the neutrino mass and hierarchy. If residual Galactic contamination in the CMB spectrum is well constrained, a PIXIE-like experiment may probe magnetic moments down to $\kappa \lesssim 3 \times 10^{-11}\ \mu_B$ for the 13 and 23 modes. While still 1 order of magnitude weaker than constraints from stellar physics [12–14], such a constraint would be competitive with current lab-based constraints from ν–e scattering measurements [10,11]. Further improvements in sensitivity, as proposed by the PRISM experiment [34], would lead to still stronger bounds on the neutrino lifetime and magnetic moment, making precision CMB spectral measurements a competitive and complementary tool for probing new physics in the neutrino sector.

ACKNOWLEDGMENTS

This work is supported partly by GRAPPA Institute at the University of Amsterdam (S. A. and B. J. K.) and JSPS KAKENHI Grant No. JP17H04836 (S. A.). This project has been carried out in the context of the "ITFA Workshop" course, which is part of the joint bachelor program in Physics and Astronomy of the University of Amsterdam and the Vrije Universiteit Amsterdam, for bachelor students (J. L. A., W. M. B., E. B., J. B., S. B., G. L., M. R., D. R. v. A., and H. V.). The actual work was done in three independent groups A, C, and D (group B did not survive) during a four-week period of January 2018. The group A (E. B., G. L., and H. V.) worked on theoretical calcluations of neutrino decay and absorption, having contributed to Secs. II A and II C and made Figs. 1–3. The group C (J. L. A., J. B., and M. R.) worked on the COBE-FIRAS data analysis and contributed to Sec. III including Figs. 4–6. The group D (W. M. B., S. B., and D. R. v. A.) made future projection for PIXIE, having contributed to Sec. IV including Figs. 8 and 9. In addition, all the groups gave substantial contributions to Sec. I by studying the relevant literature for each subject.

APPENDIX: EMISSIVITY OF PHOTONS

In this section, we derive exact formulas for decay and absorption intensities without making any assumptions.

1. Decay

From kinematics of the decay $\nu_j \to \nu_i + \gamma$, one obtains

$$p_\gamma = p_\gamma^d(p_\nu, \mu) \equiv \frac{\Delta m_{ij}^2}{2\left(\sqrt{p_\nu^2 + m_j^2} - p_\nu \mu\right)}, \tag{A1}$$

where $p_\nu = |\boldsymbol{p}_\nu|$; $p_\gamma = |\boldsymbol{p}_\gamma|$; $\boldsymbol{p}_\nu$ and $\boldsymbol{p}_\gamma$ are the momentum of ν_j and γ, respectively; and $\mu = \boldsymbol{p}_\nu \cdot \boldsymbol{p}_\gamma / (p_\nu p_\gamma)$. Alternatively, rewriting Eq. (A1) for μ gives

$$\mu = \mu_d(p_\gamma, p_\nu) \equiv \sqrt{1 + \frac{m_j^2}{p_\nu^2}} - \frac{\Delta m_{ij}^2}{2 p_\nu p_\gamma}. \tag{A2}$$

For the decay to happen, the variables and parameters $(p_\nu, p_\gamma, m_j, \Delta m_{ij}^2)$ have to satisfy $\mu_d^2 < 1$. The momentum of the final-state neutrino ν_i is then obtained as

$$p_{\nu_i}^d(p_\gamma, p_\nu) = \sqrt{p_\gamma^2 + p_\nu^2 - 2 p_\gamma p_\nu \mu_d(p_\gamma, p_\nu)}. \tag{A3}$$

The photon emissivity at energy p_γ is obtained as an equation similar to Eq. (14) but by replacing the neutrino number density with the neutrino phase space density integrated over momentum space,

$$\begin{aligned} P_{\rm dec}(p_\gamma) &= \frac{g_\nu}{(2\pi)^2} \int \frac{d^3 p_\nu}{e^{p_\nu / T_\nu} + 1} \frac{m_j \Gamma}{\sqrt{p_\nu^2 + m_j^2}} \\ &\quad \times p_\gamma \delta(p_\gamma - p_\gamma^d(p_\nu, \mu))(1 + f_{\rm CMB}(p_\gamma)) \\ &\quad \times \left[1 - \frac{1}{e^{p_{\nu_i}^d(p_\gamma, p_\nu)/T_\nu} + 1}\right], \\ &= \frac{\Gamma m_j \Delta m_{ij}^2}{4\pi^2} \frac{1 + f_{\rm CMB}(p_\gamma)}{p_\gamma} \\ &\quad \times \int_0^\infty \frac{dp_\nu p_\nu}{(e^{p_\nu/T_\nu} + 1)\sqrt{p_\nu^2 + m_j^2}} \\ &\quad \times \left[1 - \frac{1}{e^{p_{\nu_i}^d(p_\gamma, p_\nu)/T_\nu} + 1}\right] \\ &\quad \times \int_{-1}^{1} d\mu \delta(\mu - \mu_d(p_\gamma, p_\nu)), \end{aligned} \tag{A4}$$

where $g_\nu = 2$ is the number of helicities of the neutrino, the lifetime of ν_j is longer than its proper lifetime τ by a Lorentz factor of $(p_\nu^2 + m_j^2)^{1/2}/m_j$, the stimulated emission is taken into account with the term $1 + f_{\rm CMB}(p_\gamma)$, and the term in the square brackets represents the Pauli blocking for the final neutrino state with momentum $p^d_{\nu_i}$. In the second equality, we changed the δ function of p_γ to that of μ, by using $\delta(p_\gamma - p_\gamma^d) = |\partial p_\gamma^d/\partial\mu|^{-1}\delta(\mu - \mu_d)$ and $|\partial p_\gamma^d/\partial\mu| = 2p_\gamma^2 p_\nu/\Delta m_{ij}^2$.

The μ integral over its δ function gives a nonzero value (i.e., 1) only if $\mu_d^2 < 1$. By rearranging Eq. (A2), we find the condition to be equivalent to $x > |t - t^{-1}|y/2$, where $x = p_\nu/T_\nu$, $y = m_j/T_\nu$ and $t = 2p_\gamma m_j/\Delta m_{ij}^2$. We also note $\mu_d = [(x^2 + y^2)^{1/2} - y/t]/x$.

Finally, we evaluate the emissivity at redshift z and the observed energy of ϵ_γ. We can use all the equations derived thus far with replacements $p_\gamma \to (1+z)\epsilon_\gamma$, $p_\nu \to (1+z)p_\nu$, and $T_\nu \to (1+z)T_\nu$. The emissivity of the neutrino decay is then obtained as Eq. (19).

2. Absorption

For the absorption $\nu_i + \gamma \to \nu_j$, the kinematics relations are

$$p_\gamma = p_\gamma^a(p_\nu, \mu) \equiv \frac{\Delta m_{ij}^2}{2(\sqrt{p_\nu^2 + m_i^2} - p_\nu\mu)}, \tag{A5}$$

$$\mu = \mu_a(p_\gamma, p_\nu) \equiv \sqrt{1 + \frac{m_i^2}{p_\nu^2}} - \frac{\Delta m_{ij}^2}{2p_\nu p_\gamma}, \tag{A6}$$

where p_ν is (the norm of) the momentum of ν_i; definitions of the other quantities are the same as the case of decay. The momentum of the final-state neutrino ν_j is then

$$p^a_{\nu_j}(p_\gamma, p_\nu) = \sqrt{p_\gamma^2 + p_\nu^2 + 2p_\gamma p_\nu \mu_a(p_\gamma, p_\nu)}. \tag{A7}$$

The center-of-mass energy of the initial state E is given by $E^2 = m_i^2 + 2p_\gamma[(p_\nu^2 + m_i^2)^{1/2} - p_\nu\mu]$, and the δ function of E can be replaced with that of μ through $\delta(E - m_j) = |\partial E/\partial\mu|^{-1}\delta(\mu - \mu_a)$ with $|\partial E/\partial\mu| = p_\gamma p_\nu/m_j$. The absorption cross section [Eq. (5)] then becomes

$$\sigma(p_\gamma, p_\nu, \mu) = \frac{4\pi^2 m_j^3 \Gamma}{(\Delta m_{ij}^2)^2 p_\gamma p_\nu}\delta(\mu - \mu_a). \tag{A8}$$

The absorption emissivity is given as a product of the phase space densities of both γ and ν_i, multiplied by the absorption cross section as

$$\begin{aligned} P_{\rm abs}(p_\gamma)dp_\gamma = &-p_\gamma \frac{g_\gamma}{(2\pi)^3} f_{\rm CMB}(p_\gamma) d^3p_\gamma \\ &\times \frac{g_\nu}{(2\pi)^3}\int \frac{d^3p_\nu}{e^{p_\nu/T_\nu} + 1}\sigma(p_\gamma, p_\nu, \mu) \\ &\times \left[1 - \frac{1}{e^{p^a_{\nu_j}(p_\gamma, p_\nu)/T_\nu} + 1}\right], \end{aligned} \tag{A9}$$

where $g_\gamma = 2$ is the number of polarization states of the photon. Using Eq. (A8) and performing the μ integral over the δ function that yields a nonzero value only when $\mu_a^2 < 1$, one obtains

$$\begin{aligned} P_{\rm abs}(p_\gamma) = &-\frac{2}{\pi^2}\frac{m_j^3\Gamma}{(\Delta m_{ij}^2)^2} p_\gamma^2 f_{\rm CMB}(p_\gamma) \\ &\times \int_0^\infty \frac{dp_\nu p_\nu}{e^{p_\nu/T_\nu} + 1}\Theta(1 - \mu_a^2(p_\gamma, p_\nu)) \\ &\times \left[1 - \frac{1}{e^{p^a_{\nu_j}(p_\gamma, p_\nu)/T_\nu} + 1}\right], \end{aligned} \tag{A10}$$

where Θ is the Heaviside step function. As in the case of decay, this constraint, $\mu_a^2 < 1$, is equivalent to $x > |t - t^{-1}|y/2$, with $x = p_\nu/T_\nu$, $y = m_i/T_\nu$ and $t = 2p_\gamma m_i/\Delta m_{ij}^2$.

Lastly, with replacements $p_\gamma \to (1+z)\epsilon_\gamma$, $p_\nu \to (1+z)p_\nu$, $T_{\rm CMB} \to (1+z)T_{\rm CMB}$, and $T_\nu \to (1+z)T_\nu$, we arrive at Eq. (20).

[1] C. Patrignani *et al.* (Particle Data Group Collaboration), Chin. Phys. C **40**, 100001 (2016).
[2] C. Giganti, S. Lavignac, and M. Zito, Prog. Part. Nucl. Phys. **98**, 1 (2018).
[3] X. Qian and P. Vogel, Prog. Part. Nucl. Phys. **83**, 1 (2015).
[4] C. Hagedorn, R. N. Mohapatra, E. Molinaro, C. C. Nishi, and S. T. Petcov, Int. J. Mod. Phys. A **33**, 1842006 (2018).
[5] M. J. Levine, Nuovo Cimento A **48**, 67 (1967).
[6] V. K. Cung and M. Yoshimura, Nuovo Cimento A **29**, 557 (1975).
[7] P. B. Pal and L. Wolfenstein, Phys. Rev. D **25**, 766 (1982).
[8] K. Fujikawa and R. E. Shrock, Phys. Rev. Lett. **45**, 963 (1980).
[9] S. L. Glashow, J. Iliopoulos, and L. Maiani, Phys. Rev. D **2**, 1285 (1970).

[10] A. G. Beda, V. B. Brudanin, V. G. Egorov, D. V. Medvedev, V. S. Pogosov, E. A. Shevchik, M. V. Shirchenko, A. S. Starostin, and I. V. Zhitnikov, Phys. Part. Nucl. Lett. **10**, 139 (2013).
[11] M. Agostini *et al.* (Borexino Collaboration), Phys. Rev. D **96**, 091103 (2017).
[12] G. G. Raffelt, Phys. Rev. Lett. **64**, 2856 (1990).
[13] G. G. Raffelt, Phys. Rep. **320**, 319 (1999).
[14] S. Arceo-Díaz, K. P. Schröder, K. Zuber, and D. Jack, Astropart. Phys. **70**, 1 (2015).
[15] A. Studenikin, J. Phys. Conf. Ser. **718**, 062076 (2016).
[16] A. Studenikin, European Physical Society Conference on High Energy Physics (EPS-HEP 2017) Venice, Italy, 2017, arXiv:1801.08887.
[17] R. Shrock, Phys. Rev. D **9**, 743 (1974).
[18] B. W. Lee and R. E. Shrock, Phys. Rev. D **16**, 1444 (1977).
[19] R. E. Shrock, Nucl. Phys. **B206**, 359 (1982).
[20] H. Georgi and L. Randall, Phys. Lett. B **244**, 196 (1990).
[21] S. Davidson, M. Gorbahn, and A. Santamaria, Phys. Lett. B **626**, 151 (2005).
[22] N. F. Bell, V. Cirigliano, M. J. Ramsey-Musolf, P. Vogel, and M. B. Wise, Phys. Rev. Lett. **95**, 151802 (2005).
[23] N. F. Bell, M. Gorchtein, M. J. Ramsey-Musolf, P. Vogel, and P. Wang, Phys. Lett. B **642**, 377 (2006).
[24] J.-M. Frère, J. Heeck, and S. Mollet, Phys. Rev. D **92**, 053002 (2015).
[25] M. Lindner, B. Radovčić, and J. Welter, J. High Energy Phys. 07 (2017) 139.
[26] P. A. R. Ade *et al.* (Planck Collaboration), Astron. Astrophys. **594**, A13 (2016).
[27] A. Gando *et al.* (KamLAND-Zen Collaboration), Phys. Rev. Lett. **117**, 082503 (2016); **117**, 109903(A) (2016).
[28] A. Mirizzi, D. Montanino, and P. D. Serpico, Phys. Rev. D **76**, 053007 (2007).
[29] D. J. Fixsen, E. S. Cheng, J. M. Gales, J. C. Mather, R. A. Shafer, and E. L. Wright, Astrophys. J. **473**, 576 (1996).
[30] D. J. Fixsen and J. C. Mather, Astrophys. J. **581**, 817 (2002).
[31] E. Masso and R. Toldra, Phys. Rev. D **60**, 083503 (1999).
[32] A. Kogut, D. J. Fixsen, D. T. Chuss, J. Dotson, E. Dwek, M. Halpern, G. F. Hinshaw, S. M. Meyer, S. H. Moseley, M. D. Seiffert, D. N. Spergel, and E. J. Wollack, J. Cosmol. Astropart. Phys. 07 (2011) 025.
[33] J. Chluba and D. Jeong, Mon. Not. R. Astron. Soc. **438**, 2065 (2014).
[34] P. Andre *et al.* (PRISM Collaboration), arXiv:1306.2259.
[35] J. A. Peacock, *Cosmological Physics* (Cambridge University Press, Cambridge, England, 1999).
[36] Y. Y. Y. Wong, Annu. Rev. Nucl. Part. Sci. **61**, 69 (2011).
[37] Y. B. Zeldovich and R. A. Sunyaev, Astrophys. Space Sci. **4**, 301 (1969).
[38] G. G. Raffelt, *Stars as Laboratories for Fundamental Physics* (University of Chicago, Chicago, 1996).
[39] W. Hu, D. Scott, and J. Silk, Phys. Rev. D **49**, 648 (1994).
[40] A. Refregier, E. Komatsu, D. N. Spergel, and U.-L. Pen, Phys. Rev. D **61**, 123001 (2000).
[41] S. P. Oh, A. Cooray, and M. Kamionkowski, Mon. Not. R. Astron. Soc. **342**, L20 (2003).
[42] W. Hu and J. Silk, Phys. Rev. D **48**, 485 (1993).
[43] J. Chluba, Mon. Not. R. Astron. Soc. **436**, 2232 (2013).
[44] R. A. Sunyaev and Y. B. Zeldovich, Astrophys. Space Sci. **7**, 3 (1970).
[45] W. Hu and J. Silk, Phys. Rev. Lett. **70**, 2661 (1993).
[46] M. H. Abitbol, J. Chluba, J. C. Hill, and B. R. Johnson, Mon. Not. R. Astron. Soc. **471**, 1126 (2017).
[47] A. Kogut, D. J. Fixsen, D. T. Chuss, J. Dotson, E. Dwek, M. Halpern, G. F. Hinshaw, S. M. Meyer, S. H. Moseley, M. D. Seiffert, D. N. Spergel, and E. J. Wollack, J. Cosmol. Astropart. Phys. 07 (2011) 025.
[48] M. Agostini *et al.* (Borexino Collaboration), Phys. Rev. D **96**, 091103 (2017).